The Long Term Corrosion Performance of Alloy 22 in Heated Brine Solutions

D.G Enos[1], C.R.Bryan[2]
[1]Materials Reliability Department
[2]Storage and Transportation Department
Sandia National Laboratories
Albuquerque, NM 87185

Abstract

Long term corrosion experiments were performed previously on Hastelloy Alloy C-22 (UNS N06022), a Ni-Cr-Mo-W alloy, in a series of heated brines formulated to represent evaporatively concentrated ground water, to evaluate the long term corrosion performance of the material.[1] However, errors in sample preparation, contamination of the experimental systems with organic materials, and other experimental issues[2] have been identified that raised concerns regarding the corrosion data generated through that previous study. In an effort to verify the conclusions of that experimental program, a series of validation tests were performed. In these tests, Alloy 22 samples were prepared and then placed in a suite of chloride-bearing brines matching those used in the original experiments. These solutions included 0.5M NaCl, simulated acidified ground water (SAW), and simulated concentrated ground water (SCW).

Under conditions where Alloy 22 is anticipated to be passive, the corrosion rate was found to be vanishingly small (i.e., below the resolution of the weight loss technique used to quantify corrosion in this study). However, under low pH conditions where Alloy 22 is anticipated to be active, or more specifically, where the chromium oxide passive film is not thermodynamically stable, the corrosion rate was appreciable. Furthermore, under such conditions the corrosion rate was observed to be a strong function of temperature, with an activation energy of 72.9 ± 1.8 kJ/mol.

In the literature, it has been argued that for some nickel alloys, as corrosion occurs, sulfur may accumulate at the metal/oxide interface with time.[3,4] The sulfur originates from within the alloy, and builds in concentration as more of the metal is consumed by the corrosion reaction. It has been asserted that such accumulation of sulfur will eventually result in the depassivation of the material. It has been clearly demonstrated by a number of researchers that the chromium and molybdenum present in engineering alloys such as Alloy 22 effectively mitigate any potential detrimental effects of sulfur accumulation[4], this is not the case for nickel alloys that do not contain such additions. In the studies performed here, SAW samples evaluated at 60 and 90°C had an appreciable corrosion rate which, given the sulfur concentration within the material, could have resulted in sulfur accumulation. Time of Flight-Secondary Ion Mass Spectroscopy (ToF-SIMS) analysis of the oxide layer revealed that while sulfur was present within the oxide for all conditions, no accumulation was observed at or near the metal/oxide interface, supporting the conclusion that this process does not affect Alloy 22.

Introduction

Long term corrosion experiments were performed previously in a series of heated brines formulated to represent evaporatively-concentrated ground water to evaluate the long term corrosion performance of Alloy 22 (UNS N06022), a Ni-Cr-Mo-W alloy. However, errors in sample preparation, contamination of the experimental systems with organic materials, and other experimental issues[2] have been identified that raise concerns regarding the corrosion data generated through that previous study. To verify the conclusions of that experimental program, a series of validation tests were performed, the results from which are discussed here. In these tests, Alloy 22 samples were prepared and then placed in the suite of chloride-bearing brines used in the previous experiments. These solutions included 0.6M NaCl,

simulated acidified ground water (SAW), and simulated concentrated ground water (SCW). The impact of each solution was evaluated at ambient temperature (approximately 23°C), 60°C, and 90°C

In prior testing, SCW was found to be the most aggressive (in terms of mass loss), followed by SAW. These results were unexpected, based upon the conventional understanding of the corrosion performance of Ni-Cr-Mo alloys. Similar to stainless steels, Ni-Cr-X based alloys such as Alloy 22 rely on the formation of a protective chromium oxide layer on the metal surface. It is the durability of this passive film which dictates the general and localized corrosion behavior of such materials. Assuming the chromium-based passive film dictates corrosion performance, the Pourbaix diagram for chromium (Figure 1) is useful in predicting Alloy 22 behavior in these solutions based on pH. The material should be passive and the corrosion rate very low in the alkaline, SCW brine. In the acidic SAW solution, the material should not be passive, and should instead undergo general corrosion at a rate consistent with the material composition. Finally, in the NaCl solution, with a pH near neutral, Alloy 22 should also be passive, with an extremely small corrosion rate. It is important to acknowledge here that the diagram for chromium, as presented in Figure 1, cannot wholly describe the behavior of a complex alloy such as Alloy 22 as it does not capture the impact of the other components of the alloy. Furthermore, the diagram in the figure is taken at 25°C, while in this study a range of temperatures were used. However, Beverskog[5] used thermodynamic data from the literature to calculate the Pourbaix diagrams for Fe-Ni-Cr alloys as a function of temperature, and found that for the chromium containing species, there were only small changes in the regions of stability when going from 25 to 100°C. As such, the diagram in Figure 1 does provide a reasonable prediction of how a material whose passivity depends on a chromium oxide will behave.

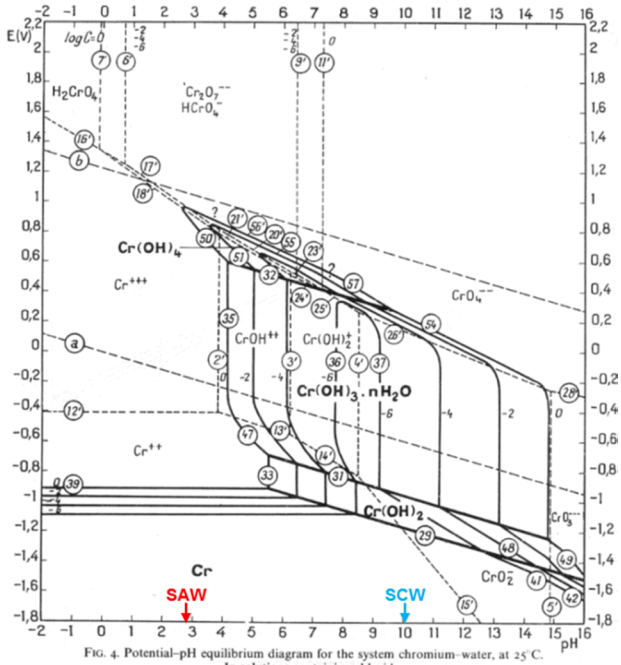

FIG. 4. Potential–pH equilibrium diagram for the system chromium–water, at 25°C. In solutions containing chloride. [Approximate representation made by considering $Cr(OH)_3 . nH_2O$.]

Figure 1: Pourbaix diagram for chromium in chloride containing solutions[6]

Experimental

The samples used to assess the general corrosion rate of Alloy 22 as a function of temperature were prepared and exposed to three different solutions at three different temperatures (ambient, 60°C, and

90°C). Specimens were removed at discrete time intervals and descaled, after which the total weight change associated with the sample was determined. The corrosion rate was then calculated based upon the total mass loss per unit area, per unit time. Weight loss measurement, while it is a classic method for evaluating the general dissolution of materials over time, is very difficult to implement on corrosion-resistant materials. Application to such materials requires meticulous weight measurement using procedures such as the NIST single substitution method, as discussed below, to address potential sources of error such as time-dependent balance drift. In addition, the uncertainties of each measurement must be assessed, such that the contributions to the measurement due to outside influences or operator-dependent biases can be removed from the data.

Environments

In order to be consistent with the earlier experiments[1], the environments considered in the present study were dictated by the solutions used previously. As such, SAW and SCW were selected. In addition, 0.5M NaCl was chosen, as it is a commonly evaluated test solution for marine applications. The SCW test solution was formulated to represent a specific well water (J-13), evaporatively concentrated by three orders of magnitude (1,000×).[7] It is slightly alkaline (pH approximately 10). The SAW test solution represents an evaporatively concentrated groundwater of a different composition, of similar ionic strength to SCW, but acidic (pH approximately 2.7) instead of alkaline.[1] The target compositions of the three solutions are listed in Table 1 below. Solution chemistry was verified at the onset and throughout the two-year experiment using ICP-OES.

Table 1: Target Solution Chemistries (M)

	0.5M NaCl	**SAW**	**SCW**
KCl	--	0.0950	0.0890
$MgSO_4$	--	0.0022	--
NaF	--	0.0141	0.0660
$NaNO_3$	--	0.3830	0.1090
Na_2SiO_3	--	0.0007	0.0007
$CaCl_2$	--	0.0020	--
$NaHCO_3$	--	--	0.6000
Na_2SO_4	--	0.4510	0.2000
NaCl	0.5000	0.5250	0.1000
NaOH	--	--	0.5000
pH	~ 7 (unadjusted)	2.7*	9.8 to 10.2*

* pH adjusted to target value with NaOH/HCl

Materials

Hastelloy Alloy C22 (UNS N06022) is known to be highly corrosion resistant in oxidizing environments. Specimens used in the previous tests were re-polished for this study. By utilizing the same material as was used in past work, any variation in performance due to compositional differences was removed. The specific composition of the samples (which were all from the same heat of material) is listed in Table 2 below:

Table 2: Composition of Alloy 22 Coupons

C	Cr	Co	Fe	Mn	Mo	Ni	P	Si	S	W	V
0.003	21.81	1.44	3.85	0.30	12.64	Bal	0.007	0.06	0.001	3.03	0.17

Each coupon was approximately 1" x 2" x 0.125" (2.54cm x 5.08cm x 0.32cm) and weighed 30g. The front and rear surfaces of each coupon were polished to a mirror finish via conventional metallographic techniques by using progressively finer grit SiC polishing paper, followed by diamond paste and the edges were mechanically ground to a 600 grit finish. Once polished, each sample was chemically cleaned. The cleaning/passivating procedure, the goal of which was to provide a uniform and reproducible surface condition for all coupons, included first degreasing in acetone, followed by a three minute soak in 15 vol% HCl. For each treatment, a single coupon was canted horizontally in a 250 mL beaker containing 200 mL of stirring acetone or HCl solution. All solutions were kept at ambient temperature. The samples were individually degreased in acetone for three minutes to remove residual machining residue, after which they were briefly submersed in deionized (DI) H_2O and blown dry using filtered, dry nitrogen. The coupons were placed in a 105 °F (40.5 °C) forced air dryer for 15 minutes to complete the drying process, and were allowed to cool before any subsequent handling. While the acetone was replenished as necessary during the degreasing process, each 200 mL 15 vol% HCl sample was used for no more than five individual coupons due to the concern of increasing aggressiveness of the solution due to metal ion buildup. After each coupon was soaked in the HCl solution for 3 minutes, the sample was immediately rinsed in a larger volume (300-400 mL) of DI H_2O. The coupon was removed and immediately placed under flowing DI H_2O for two minutes. It was then blown dry using filtered, dry nitrogen and placed in a 105 °F (40.5 °C) forced air dryer for 15 minutes.

Once cooled, the initial weight of each coupon was documented. The coupon length, width and thickness were recorded using calibrated digital calipers, and the surface area was calculated.

Immersion Testing Procedures

For the 60ºC and 90ºC tests, the exposure tanks consisted of 5 liter, o-ring sealed glass flasks. There were two flasks for each environment/temperature combination, for a total of 12 temperature controlled tanks. Each flask employed a glass cover with five ground glass joints accommodating an Allihn drip tip glass condenser, PFA fluoropolymer coated control thermocouple, aeration plumbing and access ports. Each bath is heated with an independent, feedback-controlled heating mantle. Elevated temperature baths were insulated to maintain temperature uniformity. One ambient temperature (approximately 23 °C) bath was used for each of the three environments, consisting of a rectangular glass ten-gallon tank with a domed polycarbonate cover and access holes for temperature measurement, aeration and solution replenishment.

Specimens were placed on polytetrafluoroethylene (PTFE) rods, and hung on a PTFE rack. Three groups of four coupons (1 complete rack) were placed in each of the elevated-temperature baths. As the ambient-temperature containers were larger, each one held two racks. Sample-to-sample contact was prevented by PTFE spacers between adjacent samples on each rod. This arrangement allowed a single group of specimens to be removed at each time interval without disturbing the samples remaining in the bath. Two complete racks (24 samples) were evaluated in each environment, with a total of 8 coupons being removed from each environment at each test interval. One of the coupons was for surface analysis, while the remaining 7 were used to evaluate the corrosion rate.

Specimens were removed after 3, 9, 18, and 24 months of exposure. Samples of each solution were taken when coupons were removed, and stored for later compositional analysis. The 3 month exposure was performed after the 18 month coupons were removed from the baths. (i.e., new samples were added to the sample racks after the 18-month coupons were removed). Although the condenser minimized evaporative losses, it was necessary to add deionized water periodically to ensure the solution concentrations remained constant. No other modifications to the solution chemistry were made over the course of the test. Compositional analyses verified that the solution chemistry did not drift with time.

Post Exposure Surface Analysis

Upon the completion of each exposure test time interval, a single coupon from each test condition was set aside for surface analysis and the oxide chemistry evaluated in three different locations. Aside from rinsing in deionized water, no cleaning procedures were applied to these coupons. The surfaces of this subset of coupons was observed via traditional optical microscopy to look for any signs of significant attack. Time-of-Flight Secondary Ion Mass Spectroscopy (ToF-SIMS) was used to probe the composition of the oxide layer on the surface of the Alloy 22 coupons once removed from solution. Upon the completion of each exposure test time interval, a single coupon from each test condition was set aside for surface analysis and the oxide chemistry evaluated in three different locations. Aside from rinsing in deionized water, no cleaning procedures were applied to these coupons. Due to the complexity of the oxide layer and the lack of an appropriate set of standards, exact compositions could not be reported. However, the data can be used to determine the relative concentrations and locations of various constituents within the oxide. To evaluate the oxide thickness, the less abundant ^{18}O isotope was used, rather than the more abundant ^{16}O isotope because the ^{16}O signal tended to be too large, overwhelming the detector.

Coupon Descaling

The remainder of the samples were immediately immersed in DI H_2O after removal from the exposure baths to prevent drying of the solution on the coupon surface. Each coupon was rinsed for 2 minutes in flowing DI H_2O, blown dry using filtered, dry nitrogen, and then placed in a 105 °F (40.5 °C) forced-air dryer for 15 minutes. The coupons were stored in a nitrogen cabinet throughout the entire descaling process.

All coupons underwent a minimum of three descaling cycles using 15 vol% HCl to remove any corrosion product or residual bath deposits present on the coupon surface. Between each descaling sequence, the weight of each coupon was recorded per the mass measurement procedure discussed in the following section. The first coupon weight was recorded after the coupons were removed from the baths and rinsed; this weight was termed the coupon "as removed" weight. The coupons were descaled using 15 vol% HCl and then reweighed. The descaling and weighing cycle was repeated until the cycle to cycle coupon weight change was stable to 10 μg.

The first descaling was preceded by a three-minute acetone soak to remove any organic material that might have been deposited on the surface. The coupon was immediately submerged in DI H_2O after removal from the acetone beaker, after which it was blown dry using filtered, dry nitrogen. The coupon was then placed in a 105 °F (40.5 °C) dryer for no less than 15 minutes, and allowed to cool completely. Next, coupons were descaled in 15 vol% HCl for 3 minutes. Each coupon was then immediately placed in a beaker containing DI H_2O (300-400 mL) as a pre-rinse, and then immediately (i.e., specimens did not dry between steps) rinsed under flowing DI H_2O for two minutes. The coupon was blown dry using filtered, dry nitrogen and then placed in a 105 °F (40.5 °C) dryer for no less than 15 minutes. All subsequent descaling cycles included only a 3 minute HCl soak. The HCl solutions were replaced after cleaning/descaling 5 coupons to prevent metal ion buildup and exposure of the coupons to a more aggressive environment. The DI H_2O pre-rinse bath was also replaced after 5 uses.

Mass Measurement

The weight measurements were performed following a modified National Institute of Standards and Technology (NIST) single substitution technique.[8] A high precision analytical balance combined with a precisely calibrated weight set was used for all measurements. Typical balance calibration is performed to define the linearity and eccentricity - the accuracy of the balance (e.g., accuracy of the tare value, etc.) is not defined. A precision weight set is necessary, employing a technique such as the aforementioned NIST single substitution technique, in order to achieve weight measurements with a high degree of accuracy and minimal measurement uncertainty.

Prior to performing each set of measurements, the balance was zeroed and its self-calibration routine was executed. The laboratory temperature, pressure and relative humidity were recorded at the beginning and end of each sample collection period. At the beginning and upon completion of each measurement cycle, the sample coupon weight measurements were bounded in time with calibrated weigh standard measurements to monitor and account for balance drift. The mass standards were weighed at the beginning and end of each data set collection. They were also weighed after recording the weights of every 6 coupons. If the weighing process was paused for any reason, the standards were weighed before stopping data collection and again before restarting measurement collection. Mass standards of 20, 5, and 2 grams were used to obtain total standard weights of 20, 25 and 27 grams. The set of three standard weights was chosen to account for balance linearity among coupons with a similar weight range. Each standard and coupon was weighed three times, and the average weight was used for all calculations.

Uncertainty calculations

Each weight measurement was adjusted for balance drift using the difference between a measured standard's true weight and its apparent measured weight. The standard closest to the coupon weight was used: a coupon with a weight around 24g would require use of the 25g standard weight value to compensate for balance drift. The true standard weight was obtained by calibration against NIST-traceable primary standards. The standard was weighed before and after the coupon, and once the differences between each of the measured standard values and the true standard mass were calculated, the average of the two was used to adjust the coupon weight value.

The uncertainty in the measurement for each coupon was also calculated. Both the coupon weight measurement and the standard weight measurement contribute to the coupon measurement uncertainty. The coupon weight measurement uncertainty was calculated as the standard deviation (1σ) of the three measurements recorded for each coupon. The uncertainty in the weight of the standard was obtained from calibration. The final coupon measurement uncertainly was calculated as the square root of the sum of the squares of the two uncertainties. The calculated total coupon weight loss was calculated in a similar manner, by combining the uncertainties in the initial coupon weight and the final coupon weight.

Results and Discussion

As discussed above, Alloy 22 coupons were evaluated for the mass loss due to general corrosion following exposure to chloride bearing solutions for up to two years at temperatures of 23, 60, and 90C. While a measureable dissolution rate was observed for SAW, the mass change for samples exposed to both SCW and 0.5M NaCl were below the ability of the weight loss method (as employed in this study) to detect. Below, the results for SAW are presented, followed by SCW (due to its importance in prior work). The data from the 0.5M NaCl have been omitted save for the discussion at the end of this section.

Weight Change as a Function of Temperature and Time in SAW

The corrosion rate, CR, was calculated from the weight change data as:

$$CR = \frac{\Delta W}{\rho \times SA \times t}$$

Where ΔW is the total measured weight change (i.e., initial weight – post-descaling weight), ρ is the density of Alloy 22 (8.69 g/cm^3),[9] SA is the surface area of the test coupon, and t is the total exposure time. From the equation, it is also possible to establish the minimum corrosion rate that the technique is capable of resolving, which is a function both of the accuracy of the balance and the time period of the exposure. Given the uncertainties associated with the weight measurement, the minimum measureable corrosion rates as a function of time were 5, 1.6, 0.8, and 0.6 nm/yr for the 3, 9, 18, and 24 month intervals, respectively. The average results for the SAW brine (n=7) are presented in Table 3. At ambient temperature, the corrosion rate was unresolvable using the weight-loss method as implemented in this study. At 60°C, a readily resolvable corrosion rate was observed. This rate was larger at 3 months, then

decreased and remained fairly constant for times beyond that point. The initially elevated corrosion rate at short times is consistent with the behavior of other corrosion-resistant materials. Furthermore, the constant corrosion rate with time, even at 24 months, indicates that this is a general corrosion process, as anticipated from the Pourbaix diagram. The same behavior was observed at 90°C, albeit with a corrosion rate nearly an order of magnitude larger.

It should be noted that in some cases, the magnitude of the weight change observed is on the order of the resolution of the weight-loss technique as implemented in this study. As a result, there were cases where the weight change was slightly negative, and as a result, the calculated corrosion rate is slightly negative. In such cases, while the calculated "corrosion rate" is negative, the actual rate is effectively zero.

Table 3: Corrosion Rate vs. Time for Alloy 22 in SAW

	Ambient		60°C		90°C	
	CR (nm/yr)	1 SD	CR (nm/yr)	1 SD	CR (nm/yr)	1 SD
3 months	-3.7	19.0	63.9	23.6	499.3	38.5
9 months	6.1	6.6	47.9	14.2	475.6	13.4
18 months	0.9	3.2	47.3	5.7	474.3	14.6
24 months	1.7	3.0	45.7	3.0	457.2	10.5

SD = standard deviation

The cumulative distribution function of the measured corrosion rates at ambient temperature as a function of time is presented in Figure 2. The scatter in the data was large at 3 months, and then decreased in magnitude as time progressed. This behavior is the result of the formula used to determine the corrosion rate. Given that the accuracy of the weight change measurements themselves is on the order of 30 micrograms and is independent of exposure time, as the time increases, that uncertainty in weight change represents an increasingly small uncertainty in the apparent corrosion rate. This is reflected in the calculated values presented in Table 3.

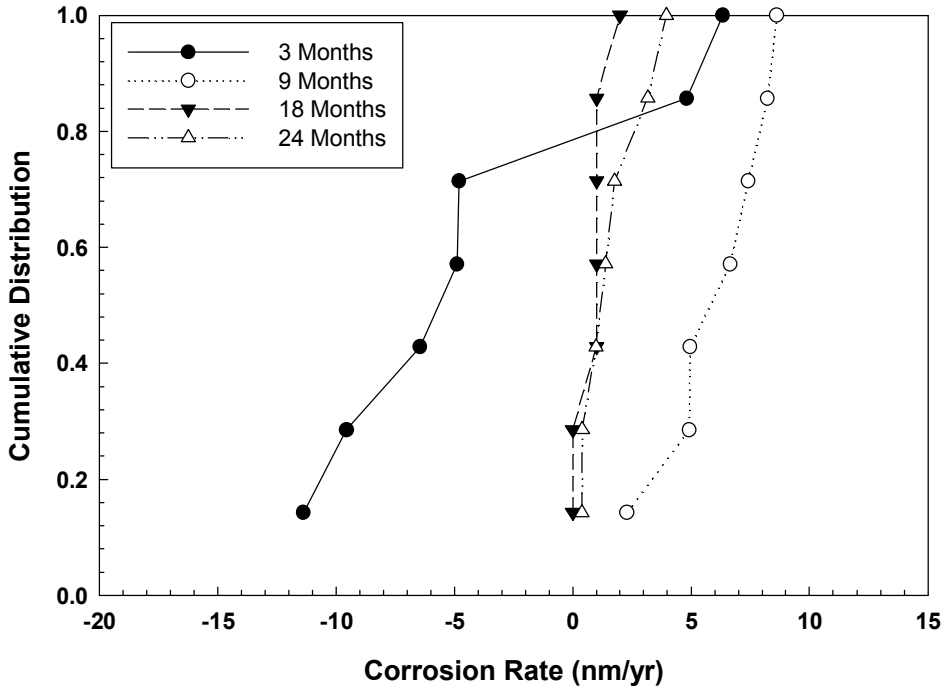

Figure 2: Cumulative distribution plots of Alloy 22 general corrosion rates for different exposure times in SAW at ambient temperature

The distribution of corrosion rates as a function of time at 60°C is presented in Figure 3. As with the ambient temperature samples, a wider distribution was observed at shorter times than at longer times. At 3 months, there was a single outlier with a corrosion rate considerably larger than the others. While evaluating the sample after the cleaning process was complete, it was noticed that there were numerous scratches in the finish. Given that the difference in weight loss between the outlier and the remainder of the population was less than 200 micrograms, it is likely that the larger weight change can be explained by the scratches, rather than an increased dissolution rate relative to the other coupons. The distributions at 18 and 24 months were nominally identical, indicating that the process was stable.

The distribution of corrosion rates as a function of time at 90°C is presented in Figure 4. As with the other temperatures, the distribution narrowed with increasing exposure time, indicating that the dissolution rate was stabilizing.

Thermal Activation Energy for General Corrosion in SAW

The distribution of corrosion rates as a function of temperature at 24 months is presented in Figure 5. In the previous long-term corrosion experiments, no environmental dependence was seen in the average general corrosion rate,[10] and furthermore, no temperature dependence of the general corrosion rate was observed when comparing data taken at 60°C and 90°C. This was inconsistent with the results obtained in this study. As illustrated in Figure 6, there is a clear temperature dependence of the general corrosion rate for Alloy 22 in SAW.

Furthermore, the data follows Arrhenius kinetics (i.e., $CR = A\,exp\left(-{E_a}/{RT}\right)$, where A is a constant, E_a the activation energy, R the gas constant, and T the temperature), as illustrated in Figure 6. By plotting the log of the corrosion rate as a function of inverse temperature, a straight line is achieved. The slope of this line is proportional to the thermal activation energy. The calculated activation energy was found to be 72.9 ± 1.8 kJ/mol.

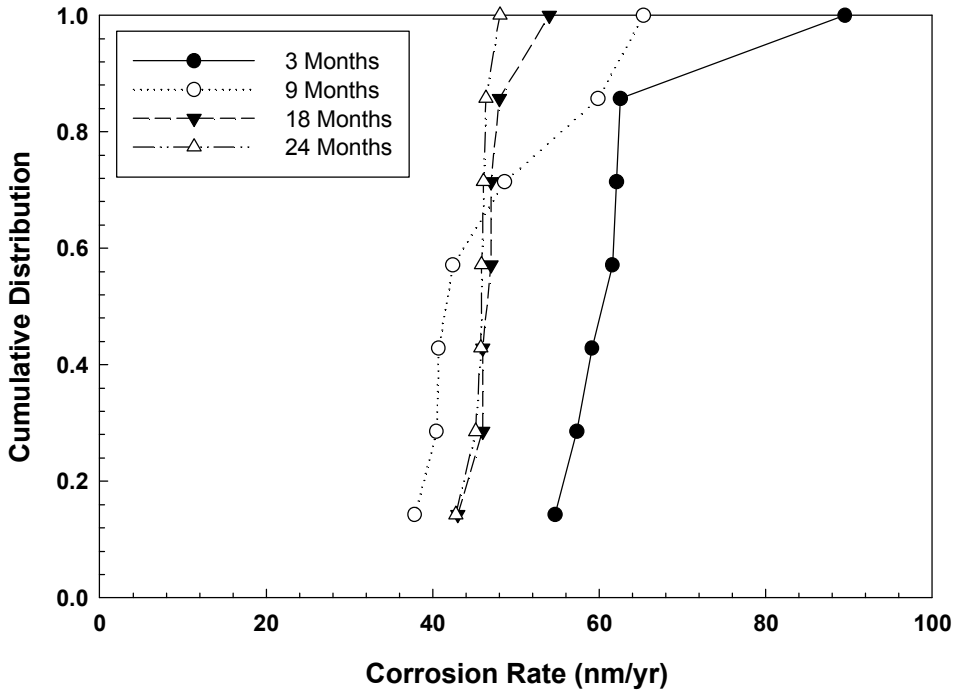

Figure 3: Cumulative distribution plots of Alloy 22 general corrosion rates for different exposure times in SAW at 60°C

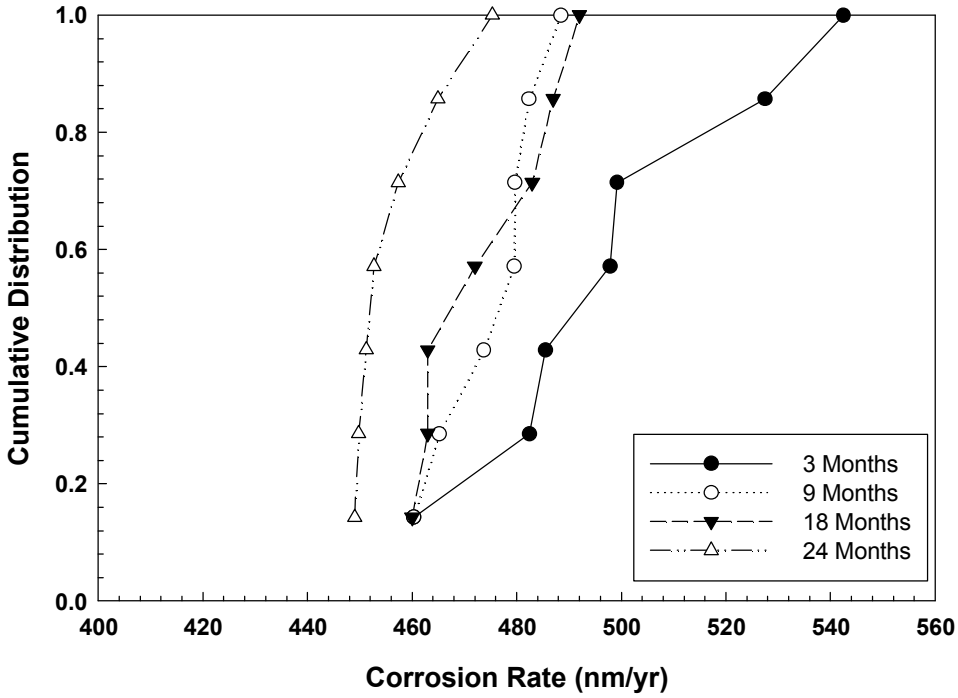

Figure 4: Cumulative distribution plots of Alloy 22 general corrosion rates for different exposure times in SAW at 90°C

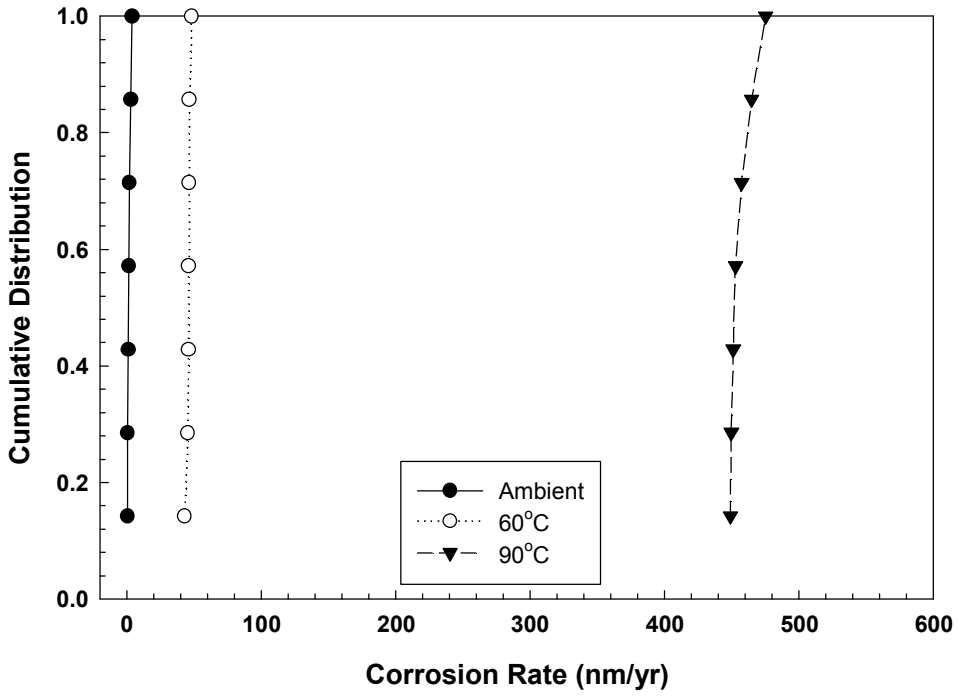

Figure 5: Cumulative distribution plots of Alloy 22 general corrosion rates for different exposure times in SAW at 24 months.

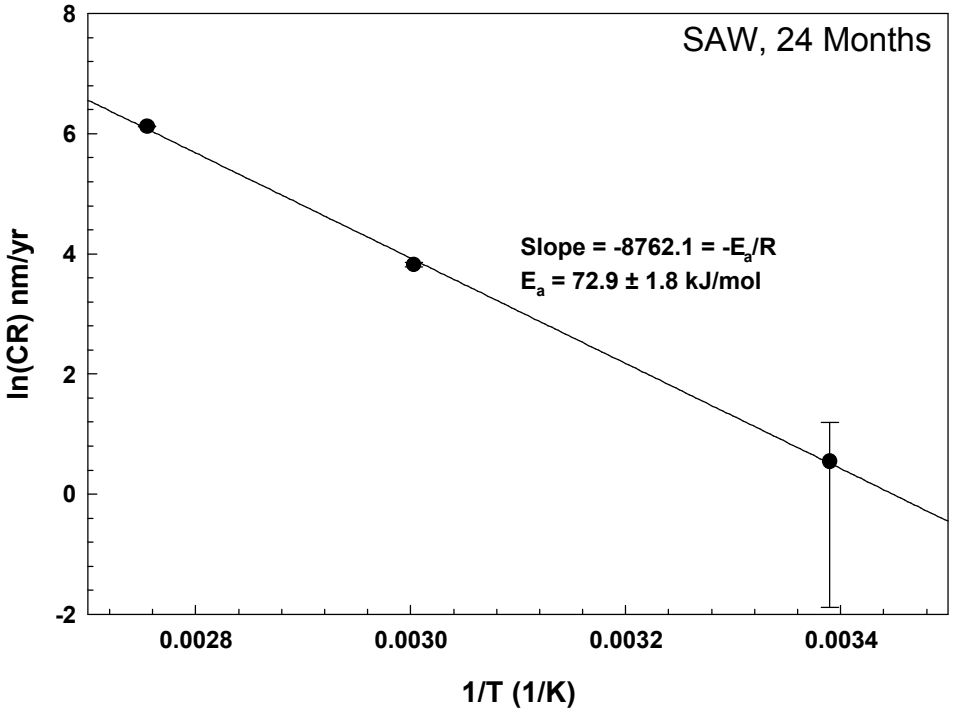

Figure 6: Activation energy calculation for samples exposed to SAW after 24 months. Based upon the data, the thermal activation energy was found to be 72.9 ± 1.8 kJ/mol. Error bars represent a single standard deviation and are shown for all three points.

Surface Morphology as a Function of Temperature and Time in SAW

In order to corroborate the weight change results, the surfaces of samples exposed at each temperature were evaluated optically. In Figure 7 it can be seen that after 24 months exposure at ambient temperature, the polishing marks were still clearly visible on the surface, indicating that little, if any, dissolution had taken place. For the sample exposed to 60°C, the polishing marks were gone, and the surface had been smoothed. In addition, some relief on the surface was visible, correlating with the underlying microstructure. This observation is consistent with the low, but readily measured, corrosion rate observed for these specimens. At 90°C, where the dissolution rate was an order of magnitude larger, the surface had been etched, revealing the underlying microstructure (grain boundaries, twins, etc.). As with the 60°C sample, the polishing marks are gone

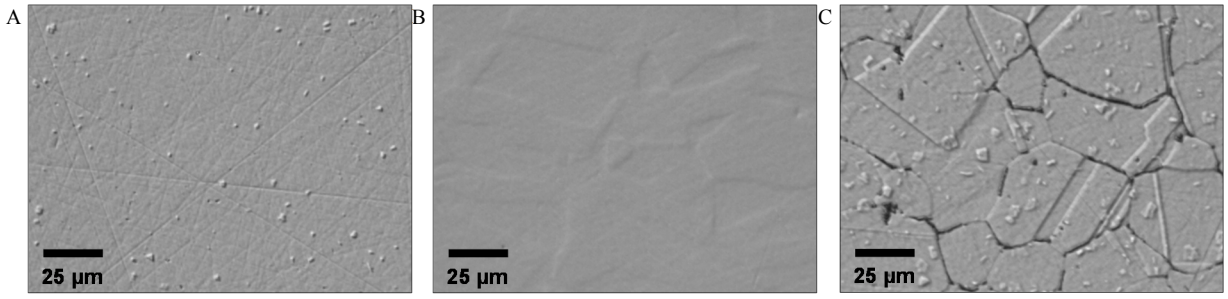

Figure 7: Surface morphology of coupons following 24 months of exposure in SAW at (a) ambient temperature, (b) 60°C, and (c) 90°C. Surface relief/contrast is due to the use of the Nomarski DIC imaging technique.

Oxide Chemistry as a Function of Temperature and Time

Time-of-Flight Secondary Ion Mass Spectroscopy (ToF-SIMS) was used to probe the composition of the oxide layer on the surface of the Alloy 22 coupons as a function of time. Upon the completion of each exposure test time interval, a single coupon from each test condition was set aside for surface analysis. Aside from rinsing in deionized water, no cleaning procedures were applied to these coupons. Due to the complexity of the oxide layer and the lack of an appropriate set of standards, exact compositions could not be reported. However, the data can be used to determine the relative concentrations and locations of various constituents within the oxide. To evaluate the oxide thickness, the less abundant ^{18}O isotope was used, rather than the more abundant ^{16}O isotope because the ^{16}O signal tended to be too large, overwhelming the detector. The ^{18}O profiles for coupons exposed to SAW as a function of temperature and time are presented in Figure 8. The sharpness of the back edge of the oxygen peak indicates that the oxide is uniform or that the surface roughness is small, and as such the thickness was taken as the depth at which the signal was 50% of the maximum level. Since the oxide layer was reasonably uniform, it was possible to determine the thickness of the oxide layer as the depth at which the signal dropped to half its maximum intensity (per ASTM E1438[11]). The oxide thicknesses determined in this manner are presented in Table 4. It should be noted that while three representative regions on each sample were analyzed, the results presented here are from a single analysis area, and while the results were similar for each location, the data presented below does not capture the variability which no doubt exists both within a single coupon or when comparing similar coupons.

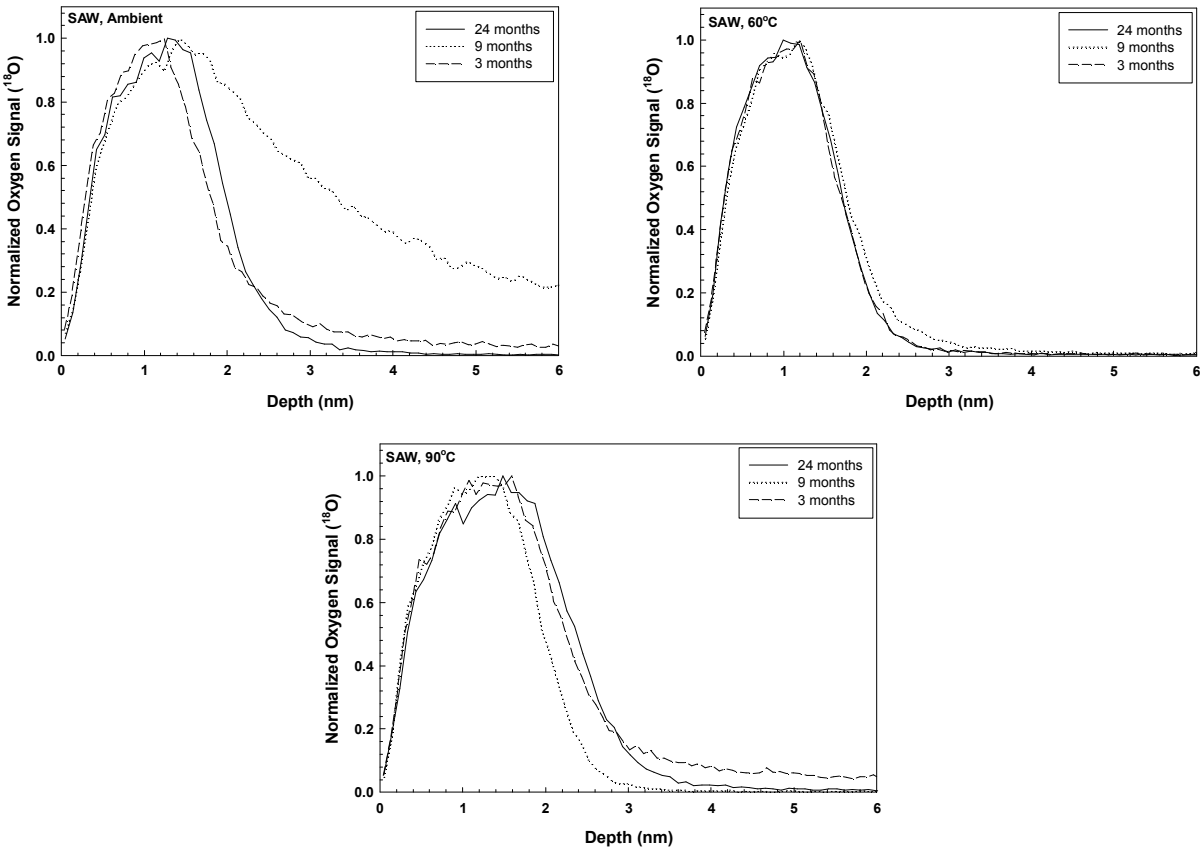

Figure 8: Oxygen-18 signal as a function of depth for Alloy 22 coupons exposed to SAW at ambient, 60°C, and 90°C.

Table 4: Oxide Thickness as a Function of Time in SAW

	Oxide Thickness (nm)		
	3 Months	9 Months	24 Months
Ambient	1.8	*	2
60°C	1.7	1.7	1.7
90°C	2.3	2	2.4

*The gradual slope of the back edge indicates that the surface was not uniform

In the literature, it has been argued that sulfur may accumulate at the bulk metal/oxide interface with time.[3] This sulfur originates from within the alloy, and builds in concentration as more of the metal is consumed by the corrosion reaction. This sulfur layer can then accelerate the dissolution rate of the alloy as well as potentially hindering the formation of a passive film. It has been demonstrated by a number of researchers that the chromium and molybdenum present in engineering alloys such as Alloy 22 effectively mitigate any potential detrimental effects,[3,4] although this is not the case for nickel alloys which do not contain such additions. In the studies performed here, we were able to assess whether sulfur accumulation occurs when Alloy 22 corrodes. SAW samples evaluated at 60 and 90°C had an appreciable corrosion rate which, given the sulfur concentration within the material (0.002 wt%), could have resulted in sulfur accumulation. ToF-SIMS analysis of the oxide layer revealed that sulfur was present within the oxide for all conditions, including the ambient temperature exposure where the corrosion rate was negligible (note that an oxide layer is always present, as it forms instantly on the metal

surface upon exposure to air). This suggests that the sulfur in the oxide was the result of the incorporation of constituents from the exposure solution (see Table 1), or through the sample preparation process. To better illustrate the location of sulfur in regions near the metal/oxide interface, the normalized intensity of oxygen and sulfur were compared for the 24 month samples, as shown in Figure 9. The absolute concentrations of oxygen and sulfur were not determined, but the relative amount of sulfur within the oxide can clearly be seen. The large peak near about 0.3 nm depth indicates sulfur on the surface of the oxide. No evidence of sulfur accumulation was observed at the metal/oxide interface for any of the samples. In ambient conditions, where no measureable corrosion has taken place, sulfur is observed within the oxide layer, decreasing to effectively zero at the metal/oxide interface. The secondary peak observed in the oxide is also seen in other coupons which underwent minimal dissolution, as will be demonstrated later for SCW and 0.5M NaCl. This observation suggests that sulfur is introduced into the oxide either through the sample preparation process, or from constituents of the exposure solution. A nearly identical result is seen at 60°C. For the 60°C samples, with an average corrosion rate of 45.7±1.6 nm/yr, no additional sulfur was built up at or near the metal/oxide interface. At 90°C, the average corrosion rate was an order of magnitude larger at 457.2±1.6 nm/yr, and as such, that much more sulfur would be available to accumulate at the metal/oxide interface. However, as with the lower temperatures, sulfur accumulation was not observed at the metal/oxide interface.

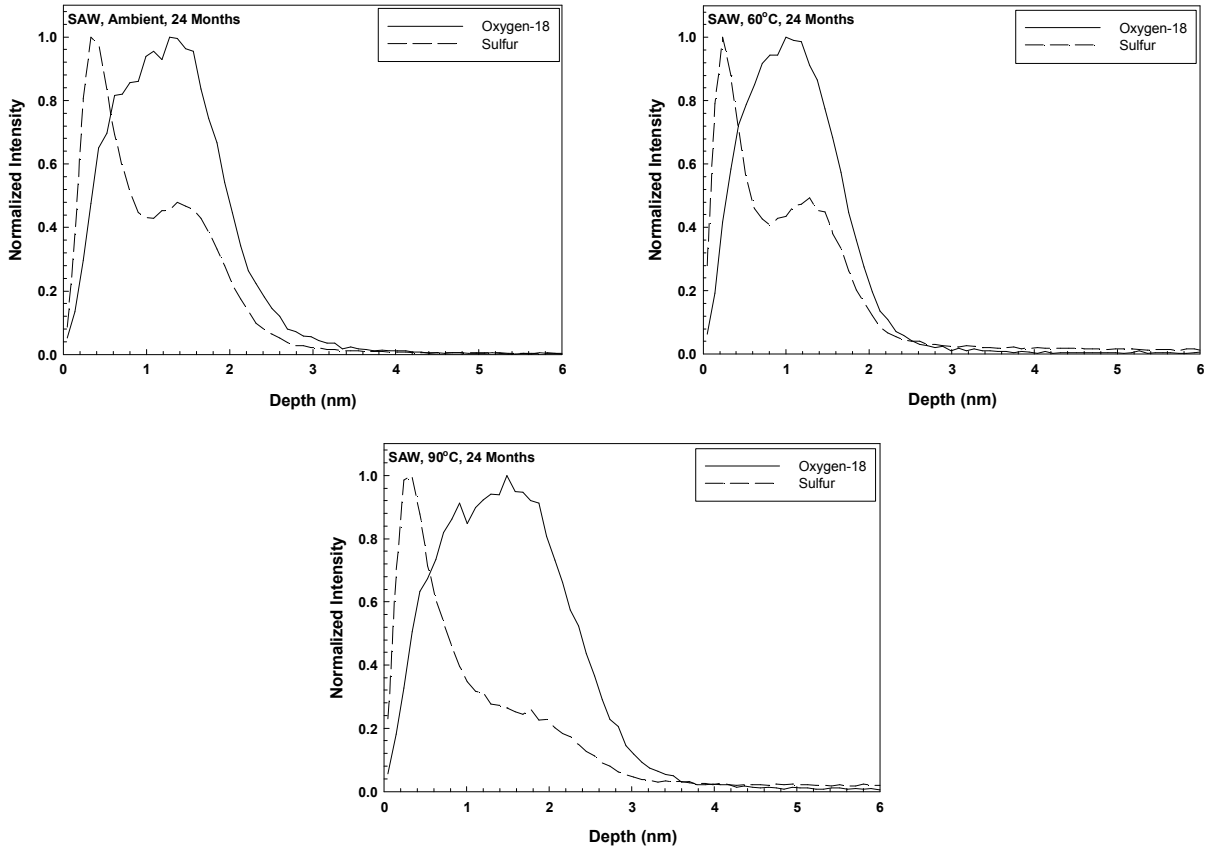

Figure 9: Comparison of the oxygen-18 and sulfur profiles through the oxide and into the metal surface for samples exposed to SAW for a period of 24 months. Data is presented as the normalized intensity for each constituent.

Based upon the results of Marcus et al.[12, 13], Mo is anticipated to bind strongly with S, forming products that are more soluble than the oxide layer, removing the sulfur from the system. In Figure **10** the concentration profile of Mo and S are presented. As can be seen, the Mo (which does not normally concentrate in the oxide or near surface metal[3]) is similar in profile to the S, supporting the assertion that the S has been bound by the Mo, and is not independently building up at the metal/oxide interface.

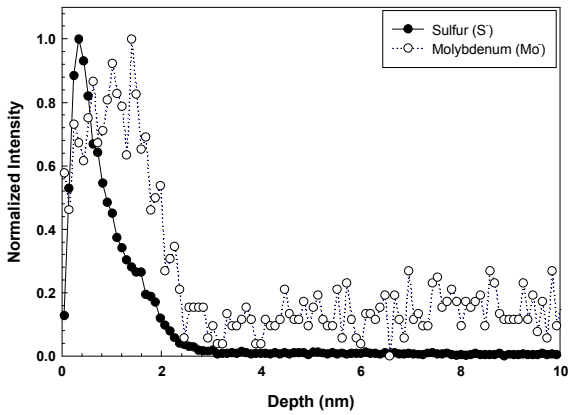

Figure 10: Normalized sulfur and molybdenum concentration through the oxide on a specimen exposed to SAW at 90C for a period of 24 months.

Weight Change as a Function of Temperature and Time in SCW

As discussed above, it was anticipated that Alloy 22 should be electrochemically passive in SCW, and as such have an extremely small dissolution rate. In all cases, the corrosion rate was effectively below the ability of the weight loss technique to detect it. One complicating factor for this solution was the observation of considerable precipitation of solution components with time, particularly at 90°C. Analysis via inductively coupled plasma optical emission spectrometry (ICP-OES) showed that the alkaline solution had leached silica from the glass exposure vessel, resulting in extensive precipitation of a sodium silicate zeolite mineral. While the deposits on the sample surfaces were not particularly tenacious, the use of mechanical means to remove them was not possible due to the potential impact of small scratches on the observed weight loss. As such the deposits had to be chemically removed. Two procedures were found to be effective in removing the deposits – soaking in a commercially available alkaline cleaner (10% aqueous solution of Brulin 815GD) or soaking in a 1M NaOH solution. Unfortunately, both of these techniques tended to remove some of the underlying material, both on blank coupons as well as the test specimens themselves. After cleaning, the final weight changes were on the order of 30 to 200 micrograms, but a similar result was observed for blank (unexposed) coupons. As such, though the results indicate a very small degree of mass loss, the weight change data from these coupons could not be reliably used to calculate the overall general corrosion rate.

As discussed for SAW, in some cases the overall weight change was below our ability to effectively resolve it, and the measured value was slightly negative resulting in a negative apparent "corrosion rate". The actual rate in such cases is effectively zero.

Oxide Chemistry as a Function of Temperature and Time in SCW

In a manner similar to that described above for SAW coupons, ToF-SIMS was used to probe the composition of the oxide layer on the surface of Alloy 22 coupons taken from the SCW baths as a function of time. The ^{18}O profiles for coupons exposed to SCW as a function of temperature and time are presented in Figure 11, and the oxide thickness as a function of exposure condition and time is presented in Table 5. The sharpness of the back edge of the oxygen peak indicates that the oxide is uniform, and as such the thickness was taken as the depth at which the signal was 50% of the maximum level. Once

again, it should be noted that the results presented here for a single analysis area do not capture the variability which no doubt exists both within a single coupon or when comparing similar coupons.

ToF-SIMS analysis of the oxide layer also revealed that sulfur was present within the oxide for all conditions, including the ambient temperature exposure, suggesting that the material in the oxide was the result of the constituents of the exposure solution or introduced during initial sample preparation. To better illustrate the location of sulfur in regions near the metal/oxide interface, the normalized intensity of oxygen and sulfur were compared for the 24 month samples, as shown in Figure 12. The absolute concentrations of oxygen and sulfur were not determined, but the relative amount of sulfur within the oxide can clearly be seen. The large peak near about 0.3 nm depth indicates sulfur on the surface of the oxide. Despite the negligible corrosion rate for all of the samples, sulfur is observed within the oxide layer, decreasing to effectively zero at the metal/oxide interface. This observation suggests that sulfur is introduced into the oxide either through the sample preparation process, or from constituents of the exposure solution. No evidence of sulfur accumulation was observed at the metal/oxide interface for any of the samples. The observation for 60°C where the oxide thickened, but the sulfur was predominantly at the surface reinforces the theory that the sulfur is due to bath constituents rather than the alloy itself.

Table 5: Oxide Thickness as a Function of Time in SCW

	Oxide Thickness (nm)		
	3 Months	9 Months	24 Months
Ambient	1.9	1.9	2.7
60°C	3.1	3.6	6.4
90°C	--	--	--

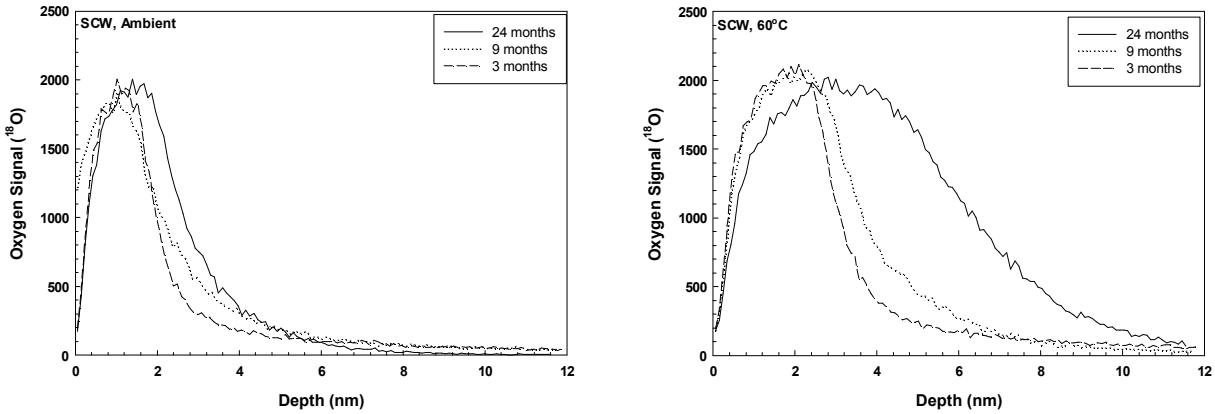

Figure 11: Oxygen-18 signal as a function of depth for Alloy 22 coupons exposed to SCW at ambient and 60°C. The 90°C samples were not analyzed due to the extensive precipitate layer present.

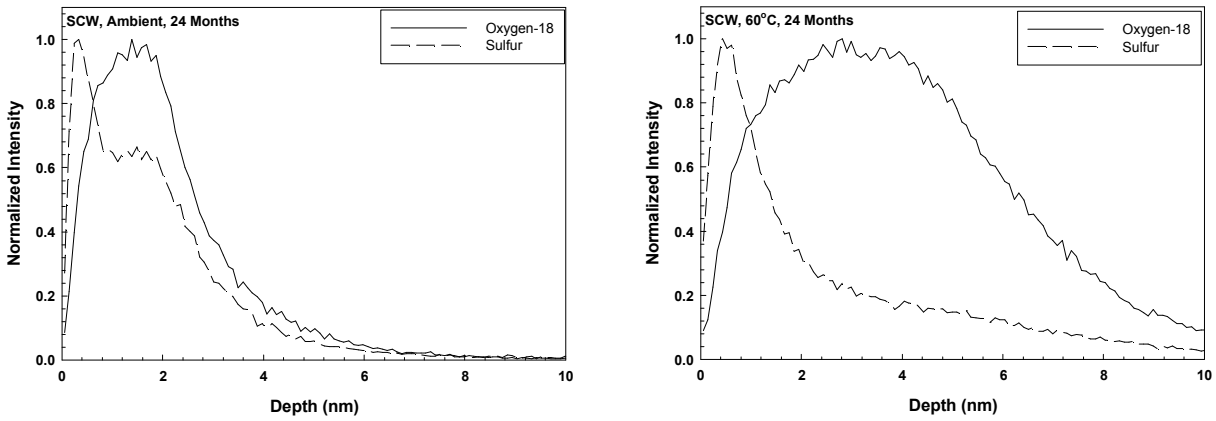

Figure 12: Comparison of the oxygen-18 and sulfur profiles through the oxide and into the metal surface for samples exposed to SCW for a period of 24 months. Data is presented as the normalized intensity for each constituent.

Summary of Weight Change and Oxide Analysis Results

In SCW and 0.5M NaCl, the general corrosion rate for Alloy 22 observed at all temperatures and all times was below the detection limit for the weight loss test used in this study (approximately 2 nm/yr). As such, while the general corrosion rate in those environments may be observed to be a function of temperature through the use of more sensitive techniques, it was not observed in this study. In SAW, however, the general corrosion rate was clearly a function of temperature.

The dataset produced in previous experimentation to determine the general corrosion rate of Alloy 22 has considerable scatter to it,[10] and the trend of the corrosion rate as a function of environment is inconsistent with any mechanistic understanding of the corrosion process. In those earlier experiments, the most aggressive condition was a slightly alkaline brine (SCW), and the low pH SAW was one of the less aggressive brines (Figure 13).

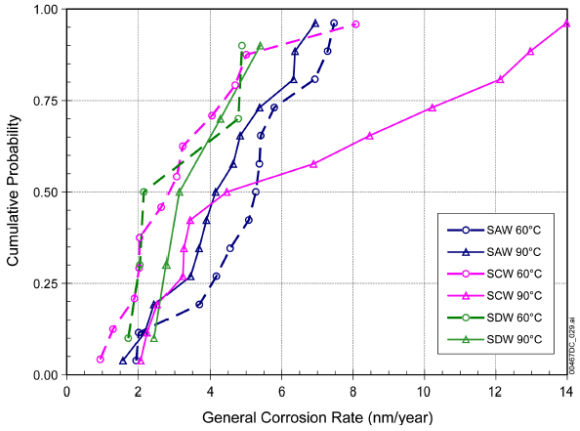

Figure 13: Corrosion rate distributions for specimens exposed for 5 years in heated brine.[10]

Similar to stainless steels, Alloy 22 and other Ni-Cr-X based alloys rely on the formation of a protective chromium oxide layer which forms on the metal surface. It is the durability of this passive film which dictates the general and localized corrosion behavior of such materials. Based upon the Pourbaix diagram for chromium in chloride-bearing solutions (which describes the thermodynamically stable species at a particular condition, but doesn't provide kinetic information), one would anticipate that the material would be passive at around pH 10 (SCW), but be undergoing general corrosion at pH levels

below 4.5 or so. So SAW, at a pH of 2.7, would be expected to be the most aggressive, while SCW at a pH of 10, would be benign.

In addition to the counterintuitive trend in corrosion rates observed in the previous work[10], the temperature dependence of the corrosion rate was also difficult to interpret from the data. Since an activation energy couldn't be extracted directly from the previous general corrosion rate data (only two temperatures were used, and due to the high variability in the results, there appeared to be no temperature dependence for that data) short term polarization resistance measurements were used to generate the corrosion rates as a function of temperature, which in turn were used to calculate the activation energy. The solutions selected were of varying nitrate to chloride ratio and in that report were considered to accurately represent what took place in the long term corrosion tests. This polarization data also had significant scatter associated with it (several orders of magnitude) as illustrated in Figure 14. Because of the large degree of scatter in the datasets, the uncertainty was very large, and the possible activation energy was estimated to be from 3.37 kJ/mol to 60.05 kJ/mol.

In an effort to address with the uncertainty in the previous dataset[10], a series of long-term tests with Alloy 22 in SAW, SCW, and 0.5M NaCl were performed. Care was taken to alleviate the concerns which existed for the previously obtained data[2] (better defined initial state, elimination of organic contamination in the bath from the disintegration of the containers and hardware, etc.) The corrosion rates measured here differ from the results obtained previously. The corrosion rates were found to be higher in the SAW, and virtually un-measureable in the SCW and NaCl solutions. These results are consistent with the general understanding of how Ni-Cr-Mo-W alloys behave in chloride-bearing solutions of varying pH. The results from the new testing are also very consistent, without the variability exhibited by the previous data.

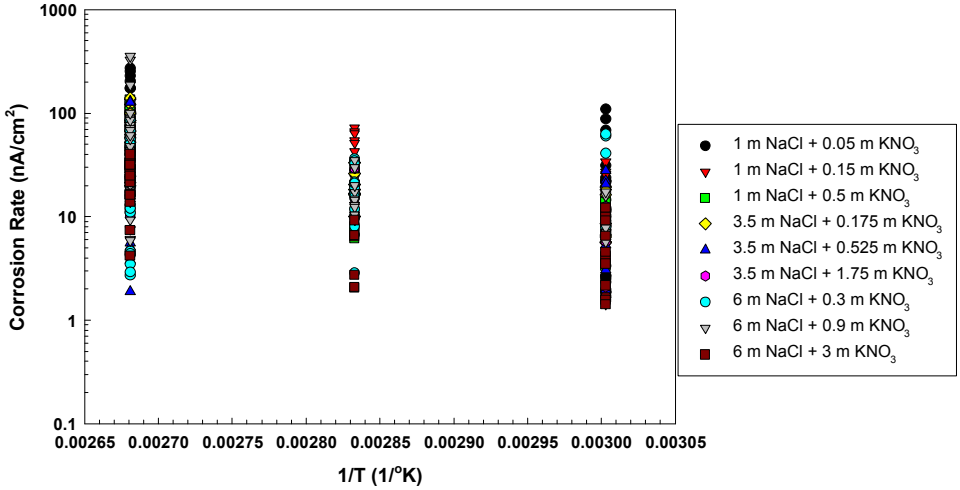

Figure 14: Corrosion rate as a function of temperature for the environments used to determine the temperature dependence of Alloy 22 in previous work in lieu of the long term general corrosion rate data.[10]

The general corrosion rates for Alloy 22 observed in this study are summarized in Table 6 for the 24 month data, which have the lowest measurement uncertainties. The corrosion behavior is clearly a strong function of environment. In the SCW and 0.5M NaCl solutions, where Alloy 22 is anticipated to be passive based upon the Pourbaix diagram for Cr in chloride bearing solutions, the corrosion rate was found to be below the resolution of the weight loss technique as implemented in this study. We know that some corrosion did occur, however, as the oxide layer was observed to thicken in both of these solutions.

Under low pH conditions in SAW, where Alloy 22 is anticipated to be active, or more specifically, where the chromium oxide passive film is not thermodynamically stable, the corrosion rate was appreciable, and the oxide layer was not observed to thicken, suggesting that it was indeed dissolving into the solution. Furthermore, under such conditions the corrosion rate was also observed to be a strong function of temperature, with an activation energy of 72.9 ± 1.8 kJ/mol.

Table 6: 24 Month Corrosion Rate as a Function of Environment

	Ambient		60°C		90°C	
	CR (nm/yr)	1 SD	CR (nm/yr)	1 SD	CR (nm/yr)	1 SD
SAW	1.7	3.0	45.7	3.0	457.2	10.5
SCW	0.3	1.9	0*	2.4	--	--
0.5M NaCl	0*	2.2	1.0	2.3	1.2	2.5

*measured weight change slightly negative

Conclusions

In an effort to address concerns over the long term corrosion rate and temperature dependence data obtained in prior studies, a series of long term immersion tests were performed on Alloy 22 in the same environments as were used previously. Based upon the results obtained, the following conclusions may be made:

- The general corrosion rate of Alloy 22 is a strong function of environment, being vanishingly small in solutions where the material is passive (i.e., pH > 4.5 or so), and becoming appreciable in low pH environments, consistent with what was predicted based upon the Pourbaix diagram for Cr in chloride-bearing solutions
- Under conditions where it could be measured, the general corrosion rate of Alloy 22 was found to be a strong function of temperature, with an activation energy of 72.9 ± 1.8 kJ/mol.
- Sulfur accumulation at the metal/oxide interface was not observed for any of the conditions evaluated in this study. However, sulfur accumulation did appear to occur at the oxide/solution interface as the oxide was removed by dissolution into the solution. The mechanism for this process is unknown.

References

1. Fix, D.V, Rebak, R.B. "*The Long-Term Corrosion Test Facility at Lawrence Livermore National Laboratory*", 2007 ASME Pressure Vessels and Piping Division Conference, July 22-26, 2007, paper PVP200726165 (also LLNL report no. UCRL-PROC-229377)
2. SNL, 2010 Addendum to General Corrosion and Localized Corrosion of the Waste Package Outer Barrier, ANL-EBS-MD-000003 Rev. 3 Ad. 01, Albuquerque, NM: Sandia National Laboratories.
3. Marcus, P. and Maurice, V. 2000. "*Passivity of Metals and Alloys*." Chapter 3 of Corrosion and Environmental Degradation. Schütze, M., ed. Volume I. Materials Science and Technology Volume 19. New York, New York: Wiley-VCH.
4. Marcus, P., ed. 2002. Corrosion Mechanisms in Theory and Practice. Second Edition, Revised and Expanded. Corrosion Technology 17. New York, New York: Marcel Dekker.
5. Beverskog, P, and Puigdomenech, I. 1999 "*Pourbaix Diagrams for the Ternary System of Iron-Chromium-Nickel*", Corrosion, Vol. 55, No. 11 (1999), pp. 1077-1087.
6. Pourbaix, M., 1974, Atlas of Electrochemical Equilibria in Aqueous Solutions, Houston, TX: NACE International.

7. McCright, R.D. 1998 *"Engineered Materials Characterization Report. Volume 3: Corrosion Data and Modeling Update for Viability Assessment*", Report UCRL-ID-119564, Vol. 3, Rev. 1. (June 30, 1998).
8. NIST SOP No. 7 "*Recommended Standard Operating Procedure for Weighing by Single Substitution Using a Single-Pan Mechanical Balance, a Full Electronic Balance, or a Balance with Digital Indications and Built- In Weights*", National Institute of Standards and Technology, 2012.
9. Haynes International, 2002 "*Hastelloy C-22 Alloy*", Haynes International Brochure #H-2019.
10. SNL, 2007 General Corrosion and Localized Corrosion of the Waste Package Outer Barrier, ANL-EBS-MD-000003 Rev. 3, Albuquerque, NM: Sandia National Laboratories.
11. ASTM, 2011 "*Standard Guide for Measuring Widths of Interfaces in Sputter Depth Profiling Using SIMS*", ASTM E1438-11, ASTM International, 2011.
12. Marcus, P, M. Moscatelli, J. Oudar "*Evidences and Characterization of a Destabilizing Effect of Molybdenum on Adsorbed Sulfur and Influence on the Passivation*", Electrochemical Society Proceedings Vol. 86-7, Surfaces, Inhibition, and Passivation, 2006, pp.281-303.
13. Marcus, P., M. Moscatelli "*The Role of Alloyed Molybdenum in the Dissolution and the Passivation of Nickel-Molybdenum Alloys in the Presence of Adsorbed Sulfur*", Journal of the Electrochemical Society, Vol 136, no 6 (1989), pp. 1634-1637.

Acknowledgements

The authors gratefully acknowledge the technical support provided by Sam Lucero for assisting with the assembly and monitoring of the exposure chambers as well as a portion of the weight change measurement, Kirsten Norman for her assistance with a portion of the weight change measurement, sample preparation, and data analysis, Carly George and Eddie Lopez for sample and solution preparation, and Alice Kilgo for her assistance with sample preparation. Sandia National Laboratories is a multi-program laboratory managed and operated by Sandia Corporation, a wholly owned subsidiary of Lockheed Martin Corporation, for the U.S. Department of Energy's National Nuclear Security Administration under contract DE-AC04-94AL85000